RSC Advances

PAPER

View Article Online
View Journal | View Issue

Cite this: *RSC Adv.*, 2025, **15**, 26201

Novel quinazoline-triazole-based *N*-hydroxybenzamides/*N*-hydroxypropenamides as HDAC inhibitors: design, synthesis, biological evaluation, and docking studies†

Nguyen Phuong Dung,‡[a] Hwa Kyung Kim,‡[b] Nguyen Thi Nga,[a] Bui Quang Cuong,[a] Da Hyeon Kang,[b] Ha Young Kim,[b] Jong Soon Kang,[c] Duong Tien Anh, *[a] Truong Thanh Tung, *[d] Sang-Bae Han*[b] and Nguyen-Hai Nam *[a]

Herein, two novel series of *N*-hydroxybenzamides and *N*-hydroxypropenamides incorporating 4-oxoquinazoline and 1,2,3-triazole scaffolds were rationally designed, synthesized, and evaluated for their Histone deacetylase (HDAC) inhibitory and anticancer activities. The synthesized hydroxamic acids were evaluated for HDAC inhibitory activity using nuclear extracts from HeLa cells. *N*-hydroxybenzamide derivatives (**7a–i**) exhibited stronger HDAC inhibition than their *N*-hydroxypropenamide counterparts (**11a–i**). Compounds **7h** (7-Br) and **7c** (7-CH_3) were the most potent inhibitors, with IC_{50} values of 0.142 and 0.146 μM, respectively, which are comparable to that of the positive control, SAHA. Structural modifications at positions 6 and 7 of the quinazoline core significantly influenced activity. For CH_3- and Br-substituted derivatives, substitution at position 7 enhanced HDAC inhibition, whereas for fluorinated derivatives, 6-F (**7e**) was more potent than 7-F (**7f**). Similar trends were observed in the *N*-hydroxypropenamide series, with some exceptions. Cytotoxicity studies against cancer cells (such as SW620 and MDA-MB-231) revealed that *N*-hydroxypropenamide derivatives generally had stronger antiproliferative effects. The 6-Cl derivatives (**7d**, **11d**) exhibited the highest cytotoxic activity, highlighting the significance of halogen substitution. Selectivity assessments against normal human lung fibroblasts (MRC-5) indicated that most compounds were more toxic to cancer cells. Notably, **7d** and **11d** induced G2/M phase arrest and apoptosis, demonstrating their potential as HDAC inhibitors with promising anticancer properties. Finally, molecular docking studies on HDAC isoforms for the **7a–i** and **11a–i** series revealed key structural features crucial for the activity of the library compounds.

Received 13th June 2025
Accepted 17th July 2025

DOI: 10.1039/d5ra04193g

rsc.li/rsc-advances

1. Introduction

Enzymes involved in the post-translational modification of histone proteins have recently emerged as promising molecular targets for cancer treatment.[1] Histone deacetylases (HDACs) catalyzed for removing acetyl groups from ε-amino of lysine residues in histones, leading to chromatin condensation and gene repression, have recently garnered significant attention in the development of novel antitumor compounds.[2,3] Furthermore, HDACs also deacetylate non-histone proteins, including the tumor suppressor p53, the Runx family, GATA transcription factor, and nuclear factor-kB.[4] To date, 18 isoforms of human HDACs have been identified and classified into two families and four classes based on their sequence similarity to yeast HDACs.[5] Class I, II, and IV HDACs are zinc-dependent enzymes and can be inhibited by substances that form chelate complexes with ion Zn^{2+}.[6]

Numerous studies have demonstrated that abnormalities in HDAC expression are closely associated with cancer pathogenesis. For instance, class I HDACs are frequently overexpressed in various cancers, including HDAC1, HDAC2, and HDAC3 in renal cell carcinoma,[7] colorectal cancer,[8] and classical Hodgkin's lymphoma[9] as well as HDAC 8 in neuroblastoma tumorigenesis.[10] In the class IIb, HDAC6 is consistently upregulated during tumor progression, whereas HDAC10 exhibits variable expression levels depending on the cancer type.[11] These

[a]*Hanoi University of Pharmacy, 13-15 Le Thanh Tong, Hanoi, Vietnam. E-mail: namnh@hup.edu.vn; anhdt@hup.edu.vn; Fax: +84-4-39332332; Tel: +84-4-39330531*

[b]*College of Pharmacy, Chungbuk National University, 194-31, Osongsaengmyung-1, Heungdeok, Cheongju, Chungbuk, 28160, Republic of Korea. E-mail: shan@chungbuk.ac.kr*

[c]*Korea Research Institute of Bioscience and Biotechnology, Cheongju, Chungbuk, Republic of Korea*

[d]*Faculty of Pharmacy, PHENIKAA University, Hanoi, 12116, Vietnam. E-mail: tung.truongthanh@phenikaa-uni.edu.vn*

† Electronic supplementary information (ESI) available. See DOI: https://doi.org/10.1039/d5ra04193g

‡ Co-first author.

findings highlight the critical role of HDACs in tumor development and underscore their potential as molecular targets for cancer therapy.

In recent years, the HDAC inhibitors such as vorinostat (2006), romidepsin (2009), belinostat (2014), and panobinostat (2015) have been approved by U.S. FDA for cancer treatment.[12] These inhibitors share a common pharmacophore consisting of three key components: a cap group, a linker, and a zinc-binding group (ZBG) (Fig. 1).[13] The cap group interacts with amino acids at the entrance of the HDAC enzyme's binding pocket, which contains hydrophobic residues.[14] A recent strategy in HDAC inhibitor design involves incorporating biologically active moieties into the cap group to enhance potency and selectivity.[15–17] The linker, positioned between the cap group and the ZBG, can adopt various structural forms, including linear, cyclic, saturated, or unsaturated configurations.[14] The ZBG coordinates with the Zn^{2+} ion in the active site of HDACs, with hydroxamic acid, present in three FDA-approved anticancer drugs, being one of the most potent ZBGs. Additionally, an extended pharmacophore model has been proposed, incorporating an additional connecting unit (CU) (Fig. 1).[18] This CU, which can include triazole, oxazole, thiazole, indanone, 2,3-dihydrobenzofuran-2-one, or uracil moieties, enhances interactions between HDAC inhibitors and the enzyme's active site.[18]

4-Oxoquinazoline is a heterocyclic scaffold with diverse biological activities, including antibacterial, antifungal, anti-HIV, antitubercular, and notably, anticancer properties.[19] Another important heterocyclic motif found in many antitumor compounds is 1,2,3-triazole,[20] which can mimic various functional groups such as esters, amides, and carboxylic acids, making it a versatile bioisostere in drug design.[21] In addition, the triazole moiety is widely used in molecular hybridization strategies.[22] The incorporation of the triazole moiety in the design of novel HDAC inhibitors has also been previously reported.[23,24] In the realm of HDAC inhibition, several FDA-approved anticancer agents, such as belinostat, panobinostat, and givinostat, incorporate *N*-hydroxybenzamide or *N*-hydroxypropenamide scaffolds, which are essential for their interaction with the HDAC active site.

Building on these insights, this study presents the rational design, synthesis, and biological screening of two novel series of *N*-hydroxybenzamides and *N*-hydroxypropenamides incorporating 4-oxoquinazoline and 1,2,3-triazole scaffolds. The incorporation of these bioactive moieties was aimed at enhancing potency, selectivity, and drug-like properties, paving the way for the development of more effective HDAC inhibitors for cancer therapy. The design rationale for these compounds is illustrated in Fig. 2.

2. Methods and compound characterizations

The full experiments, computational and biological methods are available in the ESI.†

2.1. General procedures for the synthesis of compounds 7a–i

The preparation of library compounds was depicted in Scheme 1 and 2. Compound **1** (2 mmol) was dissolved in methanol (20 mL), followed by the addition of sodium azide (10 mmol). After 8 hours of was reflux, methanol was removed under reduced pressure, and water was added. The resulting mixture was extracted with dichloromethane (3 × 30 mL). Then the dichloromethane layer was dried (*via* anhydrous sodium sulfate), and evaporated under high vacumn, yielding a white to yellowish liquid.

The mixtures of corresponding anthranilic acid (or derivatives, 2 mmol) and formamide (10 mmol, excess) were stirred at 120 °C for 8 h. After completion, the reaction mixture was poured into a sodium bicarbonate solution to induce precipitation. The precipitate was filtered, washed with water (3 times), and dried to afford quinazoline-4(3*H*)-one derivatives **4a–i**. These obtained crude intermediates were used for the next step without further purification.

Each quinazoline-4(3*H*)-one intermediates **4a–i** (1.6 mmol) was dissolved in acetone (20 mL), and potassium carbonate (3.2 mmol) was added. The mixture was refluxed with stirring for 1 hour, followed by the addition of potassium iodide (0.16 mmol) and propargyl bromide (80% w/w in toluene, 1.6 mmol). The

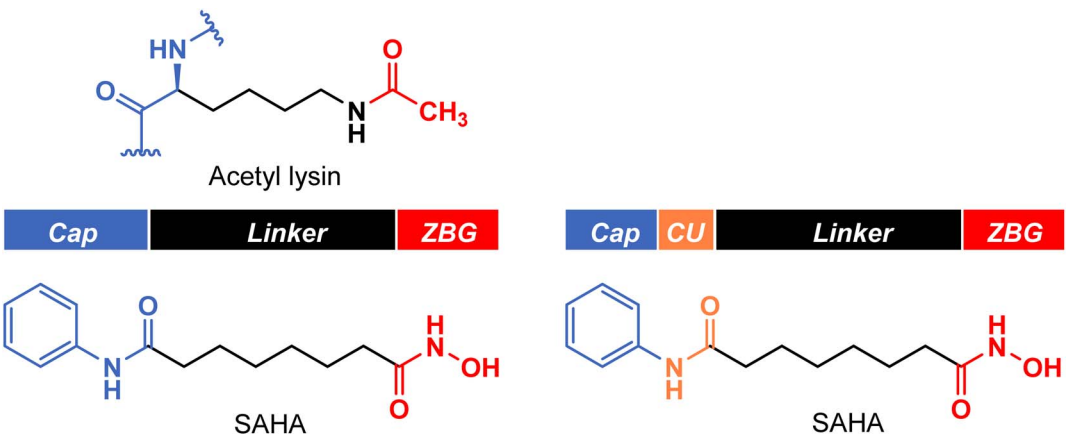

Fig. 1 Classic and extended pharmacophore model of HDACIs.

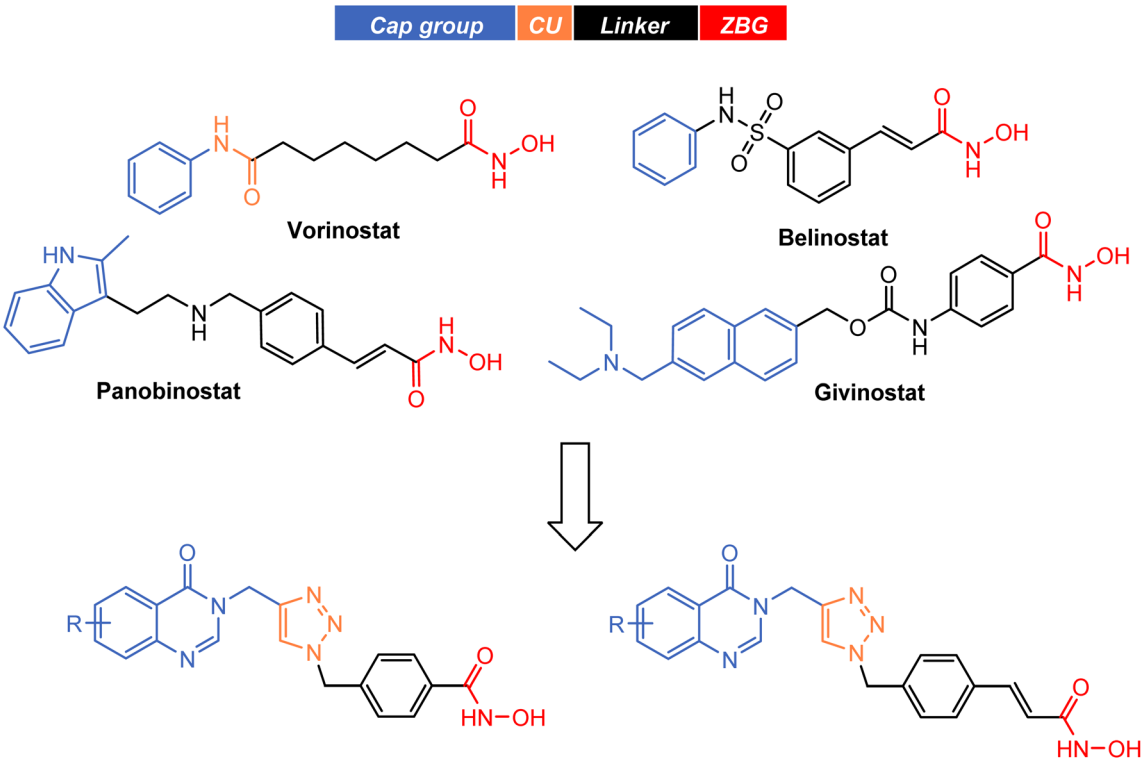

Fig. 2 Rational design of *N*-hydroxybenzamides/propenamides incorporating 4-oxoquinazoline as HDAC inhibitors and antitumor agents.

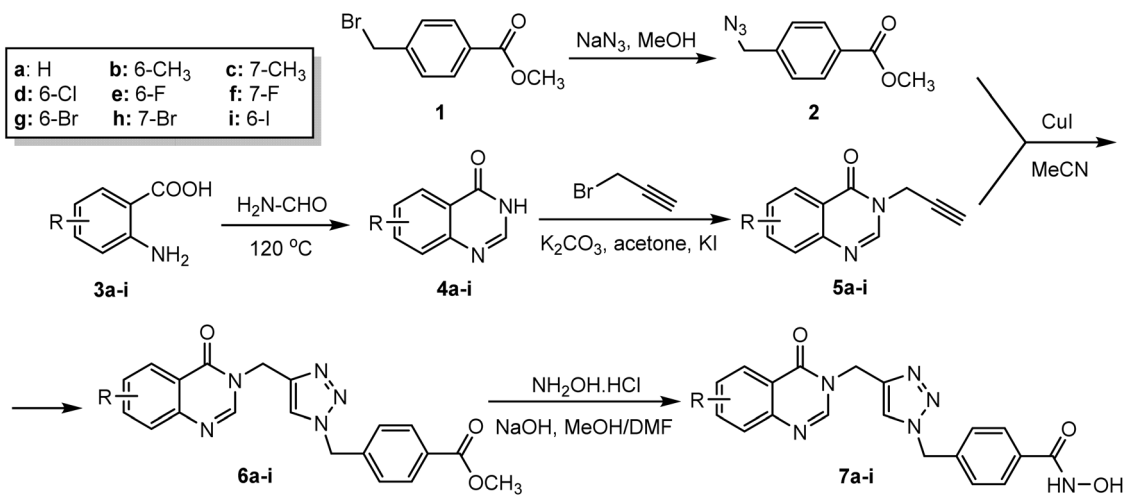

Scheme 1 Synthesis of novel *N*-hydroxybenzamides incorporating 4-oxoquinazoline.

reaction was refluxed for an additional 3 hours until completion. The solvent was then removed under reduced pressure, and water was added. The resulting mixture was extracted with dichloromethane (3 × 30 mL). The combined organic layers was dried (*via* anhydrous sodium sulfate), and evaporated under high vacumn affording white solids **5a–i**.

The propargyl intermediates **5a–i** (1.5 mmol) and compound **2** (1.5 mmol) were dissolved in acetonitrile (20 mL), followed by the addition of CuI (1.5 mmol). The reaction mixtures were refluxed for 3 hours. After completion, the solvent was removed under reduced pressure, and the residue was extracted with ethyl acetate (30 mL). The mixtures were then alkalized with a sodium carbonate solution and filtered through a Büchner funnel with Celite to remove insoluble precipitates. The organic layer was separated, while the aqueous layer was further extracted with ethyl acetate (2 × 30 mL). The combined organic extracts were dried over anhydrous sodium sulfate and concentrated under reduced pressure, yielding yellow solids **6a–i**.

Each of the esters **6a–i** (1 mmol) was dissolved in methanol (10 mL) and DMF (3 mL), then hydroxylamine hydrochloride (10 mmol) was added. The mixture was cooled to approximately 0 °

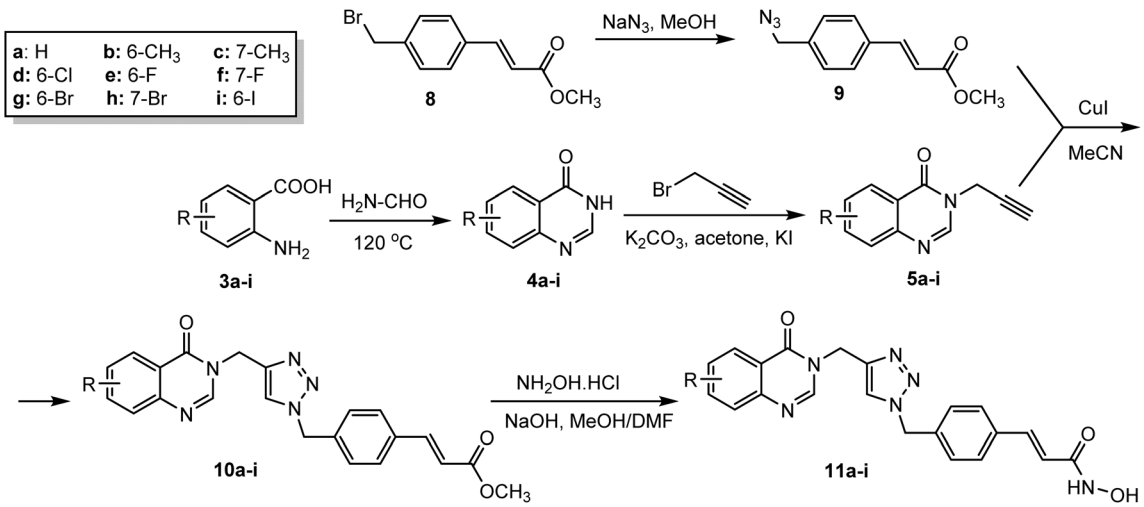

Scheme 2 Synthesis of novel *N*-hydroxypropenamides incorporating 4-oxoquinazoline.

C, and a solution of NaOH (400 mg in 1 mL of water) was added dropwise until the pH reached 11. The reaction was stirred until completion, after which the mixture was poured into ice-cold water, neutralized to pH 7, and then acidified with a dropwise addition of 5% HCl to maximize precipitation. The resulting precipitate was filtered, dried, and recrystallized from a methanol–water mixture to obtain the target compounds **7a–i**.

2.1.1 *N*-Hydroxy-4-((4-((4-oxoquinazolin-3(4*H*)-yl)methyl)-1*H*-1,2,3-triazol-1-yl)methyl)benzamide (7a). White solid; yield: 52%, mp: 191.3–192.4 °C. R_f = 0.38 (DCM : MeOH = 9 : 1). IR (KBr, cm^{-1}): 3473 (NH); 3002, 2955 (CH, arene); 2830 (CH, CH_2); 1675, 1648 (C=O); 1610, 1560 (C=C). ^{1}H NMR (500 MHz, DMSO-d_6, ppm): δ 9.10 (1H, s, OH), 8.55 (1H, s, H-2″), 8.22 (1H, s, H-5′), 8.15 (1H, dd, J = 8.00 Hz, J' = 1.50 Hz, H-5″), 7.84 (1H, td, J = 7.50 Hz, J' = 1.50 Hz, H-7″), 7.72 (2H, d, J = 8.00 Hz, H-2, H-6), 7.72–7.69 (1H, m, H-8″), 7.56 (1H, t, J = 7.00 Hz, H-6″), 7.35 (2H, d, J = 8.50 Hz, H-3, H-5), 5.61 (2H, s, ArC$\underline{H}_2$N), 5.27 (2H, s, CH_2NCO). ^{13}C NMR (125 MHz, DMSO-d_6, ppm): δ 160.37, 148.39, 143.21, 139.30, 134.96, 133.10, 128.41, 127.78, 127.74, 127.67, 126.54, 124.41, 122.06, 52.87, 41.52. HRMS (ESI) m/z calculated for: $C_{19}H_{16}N_6O_3$, $[M - H]^-$ 375.1206. Found, 375.1209.

2.1.2 *N*-Hydroxy-4-((4-((6-methyl-4-oxoquinazolin-3(4*H*)-yl)methyl)-1*H*-1,2,3-triazol-1-yl)methyl)benzamide (7b). White solid; yield: 47%, mp: 203.6–205.0 °C. R_f = 0.40 (DCM : MeOH = 9 : 1). IR (KBr, cm^{-1}): 3087, 2959 (CH, arene); 2852 (CH, CH_2); 1678, 1632 (C=O); 1608, 1534 (C=C). ^{1}H NMR (500 MHz, DMSO-d_6, ppm): δ 11.20 (1H, s, NH), 9.09 (1H, s, OH), 8.49 (1H, s, H-2″), 8.21 (1H, s, H-5′), 7.94 (1H, s, H-5″), 7.73 (2H, d, J = 8.00 Hz, H-2, H-6), 7.66 (1H, d, J = 8.00 Hz, H-7″), 7.59 (1H, d, J = 8.50 Hz, H-8″), 7.36 (2H, d, J = 8.00 Hz, H-3, H-5), 5.62 (2H, s, ArC$\underline{H}_2$N), 5.27 (2H, s, CH_2NCO), 2.44 (3H, s, CH_3). ^{13}C NMR (125 MHz, DMSO-d_6, ppm): δ 164.22, 160.30, 147.54, 146.39, 143.27, 139.32, 137.44, 136.20, 133.07, 128.41, 127.79, 127.59, 125.85, 124.39, 121.80, 52.88, 41.45, 21.29. HRMS (ESI) m/z calculated for: $C_{20}H_{18}N_6O_3$, $[M + H]^+$ 391.1519. Found, 391.1513.

2.1.3 *N*-Hydroxy-4-((4-((7-methyl-4-oxoquinazolin-3(4*H*)-yl)methyl)-1*H*-1,2,3-triazol-1-yl)methyl)benzamide (7c). White solid; yield: 49%, mp: 199.1–200.4 °C. R_f = 0.40 (DCM : MeOH = 9 : 1). IR (KBr, cm^{-1}): 3295 (OH); 3033, 2953 (CH, arene); 2856 (CH, CH_2); 1670, 1628 (C=O); 1603, 1576, 1537 (C=C). ^{1}H NMR (500 MHz, DMSO-d_6, ppm): δ 8.50 (1H, s, H-2″), 8.21 (1H, s, H-5′), 8.02 (1H, s, H-5″), 7.72 (2H, d, J = 8.50 Hz, H-2, H-6), 7.50 (1H, s, H-8″), 7.38 (1H, d, J = 8.00 Hz, H-6″), 7.35 (2H, d, J = 8.50 Hz, H-3, H-5), 5.61 (2H, s, ArC$\underline{H}_2$N), 5.24 (2H, s, CH_2NCO), 2.46 (3H, 1s, CH_3). ^{13}C NMR (125 MHz, DMSO-d_6, ppm): δ 160.25, 148.54, 148.44, 145.51, 143.27, 139.29, 133.11, 129.06, 128.40, 127.77, 127.34, 126.40, 124.41, 119.67, 52.86, 41.38, 21.77. HRMS (ESI) m/z calculated for: $C_{20}H_{18}N_6O_3$, $[M + H]^+$ 391.1519. Found, 391.1512.

2.1.4 4-((4-((6-Chloro-4-oxoquinazolin-3(4*H*)-yl)methyl)-1*H*-1,2,3-triazol-1-yl)methyl)-*N*-hydroxybenzamide (7d). White solid; yield: 44%, mp: 211.1–212.3 °C. R_f = 0.41 (DCM : MeOH = 9 : 1). IR (KBr, cm^{-1}): 3306 (OH); 3003, 2971 (CH, arene); 2831 (CH, CH_2); 1675, 1629 (C=O); 1605, 1553, 1531 (C=C). ^{1}H NMR (500 MHz, DMSO-d_6, ppm): δ 11.23 (1H, s, NH), 9.10 (1H, s, OH), 8.57 (1H, s, H-2″), 8.22 (1H, s, H-5′), 8.08 (1H, d, J = 2.00 Hz, H-5″), 7.87 (1H, dd, J = 8.75 Hz, J' = 2.25 Hz, H-7″), 7.73 (1H, d, J = 8.50 Hz, H-8″), 7.71 (2H, d, J = 8.50 Hz, H-2, H-6), 7.36 (2H, d, J = 8.00 Hz, H-3, H-5), 5.61 (2H, s, ArC$\underline{H}_2$N), 5.27 (2H, s, CH_2NCO). ^{13}C NMR (125 MHz, DMSO-d_6, ppm): δ 164.35, 159.47, 148.83, 147.06, 142.93, 139.29, 135.13, 133.01, 132.02, 130.02, 128.44, 127.80, 125.50, 124.47, 123.25, 52.90, 41.70. HRMS (ESI) m/z calculated for: $C_{19}H_{15}ClN_6O_3$, $[M + H]^+$ 411.0972, 413.0943. Found, 411.0963, 413.0977.

2.1.5 4-((4-((6-Fluoro-4-oxoquinazolin-3(4*H*)-yl)methyl)-1*H*-1,2,3-triazol-1-yl)methyl)-*N*-hydroxybenzamide (7e). White solid; yield: 45%, mp: 207.3–208.5 °C. R_f = 0.39 (DCM : MeOH = 9 : 1). IR (KBr, cm^{-1}): 3304 (OH); 3061, 3002 (CH, arene); 2844 (CH, CH_2); 1667, 1623 (C=O); 1605, 1572, 1551 (C=C). ^{1}H NMR (500 MHz, DMSO-d_6, ppm): δ 8.56 (1H, s, H-2″), 8.24 (1H, s, H-5′), 7.82 (1H, dd, J = 8.75 Hz, J' = 2.75 Hz, H-7″), 7.78 (1H, d, J = 8.50 Hz, H-8″), 7.78 (s, 1H, H-5″), 7.73 (2H, d, J = 8.00 Hz, H-2, H-6), 7.36 (2H, d, J = 8.00 Hz, H-3, H-5), 5.62 (2H, s, ArC$\underline{H}_2$N), 5.28 (2H, s, CH_2NCO). ^{13}C NMR (125 MHz, DMSO-d_6, ppm): δ 164.09, 160.75 (J_{C-F} = 245.38 Hz), 147.89, 145.30, 143.00,

139.26, 133.12, 130.71, 130.64, 128.41, 127.78, 124.47, 123.42 (J_{C-F} = 29.50 Hz), 123.35, 111.20 (J_{C-F} = 23.38 Hz), 52.88, 43.24. HRMS (ESI) *m*/*z* calculated for: $C_{19}H_{15}FN_6O_3$, $[M - H]^-$ 393.1111. Found, 393.1117.

2.1.6 4-((4-((7-Fluoro-4-oxoquinazolin-3(4*H*)-yl)methyl)-1*H*-1,2,3-triazol-1-yl)methyl)-*N*-hydroxybenzamide (7f). White solid; yield: 48%, mp: 203.9–204.6 °C. R_f = 0.39 (DCM : MeOH = 9 : 1). IR (KBr, cm^{-1}): 3314 (OH); 3043, 2959 (CH, arene); 2844 (CH, CH_2); 1665, 1621 (C=O); 1604, 1573 (C=C). ^{1}H NMR (500 MHz, DMSO-d_6, ppm): δ 8.60 (1H, s, H-2″), 8.23 (1H, s, H-5′), 8.20 (1H, dd, J = 9.00 Hz; J' = 6.50 Hz, H-5″), 7.73 (2H, d, J = 8.00 Hz, H-2, H-6), 7.50 (1H, dd, J = 10.00 Hz, J' = 2.50 Hz, H-8″), 7.42 (1H, td, J = 8.75 Hz, J' = 2.50 Hz, H-6″), 7.36 (2H, d, J = 8.00 Hz, H-3, H-5), 5.62 (2H, s, ArC$\underline{H}_2$N), 5.26 (2H, s, CH_2NCO). ^{13}C NMR (125 MHz, DMSO-d_6, ppm): δ 167.10, 164.60 (J_{C-F} = 126.00 Hz), 159.71, 150.59 (J_{C-F} = 13.13 Hz), 149.81, 143.06, 139.26, 133.14, 129.75 (J_{C-F} = 11.13 Hz), 128.41, 127.77, 124.44, 119.73, 116.27 (J_{C-F} = 23.50 Hz), 112.88 (J_{C-F} = 21.63 Hz), 52.89, 41.57. HRMS (ESI) *m*/*z* calculated for: $C_{19}H_{15}FN_6O_3$, $[M + H]^+$ 395.1268. Found, 395.1270.

2.1.7 4-((4-((6-Bromo-4-oxoquinazolin-3(4*H*)-yl)methyl)-1*H*-1,2,3-triazol-1-yl)methyl)-*N*-hydroxybenzamide(7g). White solid; yield: 51%, mp: 227.9–229.4 °C. R_f = 0.42 (DCM : MeOH = 9 : 1). IR (KBr, cm^{-1}): 3308 (OH); 3123, 3076 (CH, arene); 2989 (CH, CH_2); 1673, 1628 (C=O); 1606, 1574, 1528 (C=C). ^{1}H NMR (500 MHz, DMSO-d_6, ppm): δ 11.20 (1H, s, NH), 9.08 (1H, s, OH), 8.60 (1H, s, H-2″), 8.22 (1H, s, H-5′), 8.22 (1H, s, H-5″), 7.99 (1H, dd, J = 8.50 Hz, J' = 2.50 Hz, H-7″), 7.72 (2H, d, J = 8.00 Hz, H-2, H-6), 7.65 (1H, d, J = 9.00 Hz, H-8″), 7.35 (2H, d, J = 8.00 Hz, H-3, H-5), 5.62 (2H, s, ArC$\underline{H}_2$N), 5.27 (2H, s, CH_2NCO). ^{13}C NMR (125 MHz, DMSO-d_6, ppm): δ 159.30, 149.00, 147.41, 142.95, 139.28, 137.81, 133.10, 130.19, 128.64, 128.41, 127.78, 124.46, 123.67, 120.13, 52.89, 41.74. HRMS (ESI) *m*/*z* calculated for: $C_{19}H_{15}BrN_6O_3$, $[M + H]^+$ 455.0467, 457.0447. Found, 455.0461, 457.0442.

2.1.8 4-((4-((7-Bromo-4-oxoquinazolin-3(4*H*)-yl)methyl)-1*H*-1,2,3-triazol-1-yl)methyl)-*N*-hydroxybenzamide (7h). White solid; yield: 49%, mp: 224.3–225.9 °C. R_f = 0.42 (DCM : MeOH = 9 : 1). IR (KBr, cm^{-1}): 3307 (OH); 3065, 2988 (CH, arene); 2851 (CH, CH_2); 1664 (C=O); 1596, 1573, 1551(C=C). ^{1}H NMR (500 MHz, DMSO-d_6, ppm): δ 8.59 (1H, s, H-2″), 8.22 (1H, s, H-5′), 8.06 (1H, d, J = 8.50 Hz, H-5″), 7.92 (1H, d, J = 1.50 Hz, H-8″), 7.73–7.71 (1H, m, H-6″), 7.72 (2H, d, J = 8.50 Hz, H-2, H-6), 7.34 (2H, d, J = 8.50 Hz, H-3, H-5); 5.61 (2H, s, ArC$\underline{H}_2$N), 5.25 (2H, s, CH_2NCO). ^{13}C NMR (125 MHz, DMSO-d_6, ppm): δ 159.96, 149.81, 149.56, 142.97, 139.10, 133.34, 130.73, 130.01, 128.66, 128.53, 128.38, 127.72, 124.45, 121.21, 52.90, 41.67. HRMS (ESI) *m*/*z* calculated for: $C_{19}H_{15}BrN_6O_3$, $[M - H]^-$ 453.0311, 455.0290. Found, 453.0314, 455.0284.

2.1.9 *N*-Hydroxy-4-((4-((6-iodo-4-oxoquinazolin-3(4*H*)-yl) methyl)-1*H*-1,2,3-triazol-1-yl)methyl)benzamide (7i). White solid; yield: 42%, mp: 245.8–247.1 °C. R_f = 0.44 (DCM : MeOH = 9 : 1). IR (KBr, cm^{-1}): 3250 (NH); 3064, 2955 (CH, arene); 2850 (CH, CH_2); 1663 (C=O); 1600, 1573, 1550 (C=C). ^{1}H NMR (500 MHz, DMSO-d_6, ppm): δ 8.58 (1H, s, H-2″), 8.41 (1H, d, J = 2.00 Hz, H-5″), 8.22 (1H, s, H-5′), 8.12 (1H, dd, J = 8.50 Hz, J' = 2.00 Hz, H-7″); 7.73 (2H, d, J = 8.50 Hz, H-2, H-6), 7.49 (1H, d, J = 8.50 Hz, H-8″), 7.35 (2H, J = 8.00 Hz, H-3, H-5), 5.61 (2H, s, ArC$\underline{H}_2$N), 5.26 (2H, s, CH_2NCO). ^{13}C NMR (125 MHz, DMSO-d_6, ppm): 164.10, 159.11, 149.02, 147.69, 143.31, 142.98, 139.24, 134.81, 133.14, 129.93, 128.40, 127.78, 124.44, 123.84, 92.81, 52.89. 41.72. HRMS (ESI) *m*/*z* calculated for: $C_{19}H_{15}IN_6O_3$, $[M - H]^-$ 501.0172. Found, 501.0177.

2.2. General procedures for the synthesis of compounds 11a–i

Compounds **11a–i** were prepared following a synthetic pathway which analogous to the one used for **7a–i**, with the only difference being the replacement of methyl 4-bromomethylbenzoate for methyl (*E*)-4-bromomethylcinnamate, as illustrated in Scheme 2.

2.2.1 (*E*)-*N*-Hydroxy-3-(4-((4-((4-oxoquinazolin-3(4*H*)-yl) methyl)-1*H*-1,2,3-triazol-1-yl)methyl)phenyl)acrylamide (11a). White solid; yield: 51%, mp: 213.4–214.9 °C. R_f = 0.39 (DCM : MeOH = 9 : 1). IR (KBr, cm^{-1}): 3362 (NH); 3209 (OH); 3068, 2893 (CH, arene); 2806 (CH, CH_2); 1650 (C=O); 1607, 1546, 1514 (C=C). ^{1}H NMR (500 MHz, DMSO-d_6, ppm): δ 10.82 (1H, s, N$\underline{H}$OH), 9.11 (1H, s, O$\underline{H}$), 8.55 (1H, s, H-2‴), 8.21 (1H, s, H-5″), 8.15 (1H, dd, J = 8.00 Hz, J' = 1.00 Hz, H-5‴), 7.85 (1H, td, J = 7.75 Hz, J' = 1.50 Hz, H-7‴), 7.70 (1H, d, J = 8.50 Hz, H-8‴), 7.57 (1H, t, J = 7.00 Hz, H-6‴), 7.56 (2H, d, J = 7.5 Hz, H2′, H-6′), 7.43 (1H, d, J = 16.00 Hz, H-3), 7.33 (2H, d, J = 8.00 Hz, H-3′, H-5′), 6.46 (1H, d, J = 16.00 Hz, H-2), 5.59 (2H, s, NC$\underline{H}_2$Ph), 5.27 (2H, s, C$\underline{H}_2$NCO). ^{13}C NMR (125 MHz, DMSO-d_6, ppm): δ 163.11, 160.38, 148.36, 148.34, 143.16, 138.21, 137.47, 135.17, 134.98, 129.04, 128.33, 127.71, 126.54, 124.32, 122.01, 119.97, 52.97, 41.50. HRMS (ESI) *m*/*z* calculated for: $C_{21}H_{18}N_6O_3$, $[M - H]^-$ 401.1362. Found, 401.1368.

2.2.2 (*E*)-*N*-Hydroxy-3-(4-((4-((6-methyl-4-oxoquinazolin-3(4*H*)-yl)methyl)-1*H*-1,2,3-triazol-1-yl)methyl)phenyl) acrylamide (11b). White solid; yield: 40%, mp: 220.9–222.3 °C. R_f = 0.41 (DCM : MeOH = 9 : 1). IR (KBr, cm^{-1}): 3416 (NH); 3265 (OH); 3069, 2978 (CH, arene); 2854 (CH, CH_2); 1659, 1619 (C=O); 1603, 1514 (C=C). ^{1}H NMR (500 MHz, DMSO-d_6, ppm): δ 8.48 (1H, s, H-2‴), 8.18 (1H, s, H-5″), 7.93 (1H, s, H-5‴), 7.66 (1H, d, J = 7.50 Hz, H-7‴), 7.59 (1H, d, J = 8.00 Hz, H-8‴), 7.55 (2H, d, J = 8.00 Hz, H-2′, H-6′), 7.42 (1H, d, J = 16.00 Hz, H-3), 7.32 (2H, d, J = 8.00 Hz, H-3′, H-5′), 6.45 (1H, d, J = 16.00 Hz, H-2), 5.58 (2H, s, NC$\underline{H}_2$Ph), 5.25 (2H, s, C$\underline{H}_2$NCO), 2.44 (3H, s, C$\underline{H}_3$). ^{13}C NMR (125 MHz, DMSO-d_6, ppm): δ 163.01, 160.29, 147.55, 146.40, 143.24, 138.03, 137.47, 137.42, 136.19, 135.20, 129.04, 128.30, 127.60, 125.86, 124.28, 121.81, 120.11, 52.94, 41.44, 21.29. HRMS (ESI) *m*/*z* calculated for: $C_{22}H_{20}N_6O_3$, $[M - H]^-$ 415.1519. Found, 415.1526.

2.2.3 (*E*)-*N*-Hydroxy-3-(4-((4-((7-methyl-4-oxoquinazolin-3(4*H*)-yl)methyl)-1*H*-1,2,3-triazol-1-yl)methyl)phenyl) acrylamide (11c). White solid; yield: 47%, mp: 217.4–219.1 °C. R_f = 0.41 (DCM : MeOH = 9 : 1). IR (KBr, cm^{-1}): 3387 (NH); 3209 (OH); 2921 (CH, arene); 2857 (CH, CH_2); 1660, 1619 (C=O); 1606, 1561 (C=C). ^{1}H NMR (500 MHz, DMSO-d_6, ppm): δ 10.80 (1H, s, N$\underline{H}$OH), 9.05 (1H, s, O$\underline{H}$), 8.51 (1H, s, H-2‴), 8.19 (1H, s, H-5″), 8.02 (1H, d, J = 8.00 Hz, H-5‴), 7.54 (2H, d, J = 8.00 Hz, H-2′, H-6′), 7.50 (1H, s, H-8‴), 7.42 (1H, d, J = 16.00 Hz, H-3), 7.39

(1H, d, J = 8.50 Hz, H-6‴), 7.32 (2H, d, J = 8.00 Hz, H-3′, H-5′), 6.45 (1H, d, J = 15.50 Hz, H-2), 5.58 (2H, s, NC$\underline{H}_2$Ph), 5.24 (2H, s, C$\underline{H}_2$NCO), 2.46 (3H, s, C$\underline{H}_3$). ^{13}C NMR (125 MHz, DMSO-d_6, ppm): δ 160.24, 148.53, 148.44, 145.51, 143.4, 138.10, 137.49, 135.20, 129.06, 129.04, 128.30, 127.33, 126.40, 124.31, 120.09, 119.67, 52.94, 41.37, 21.77. HRMS (ESI) m/z calculated for: $C_{22}H_{20}N_6O_3$, $[M + H]^+$ 417.1675. Found, 417.1672.

2.2.4 (*E*)-3-(4-((4-((6-Chloro-4-oxoquinazolin-3(4*H*)-yl) methyl)-1*H*-1,2,3-triazol-1-yl)methyl)phenyl)-*N*-hydroxyacrylamide (11d). White solid; yield: 43%, mp: 233.7–235.1 °C. R_f = 0.43 (DCM : MeOH = 9 : 1). IR (KBr, cm^{-1}): 3198 (OH); 3062, 2922 (CH, arene); 2851 (CH, CH_2); 1661 (C=O); 1600, 1557 (C=C). ^{1}H NMR (500 MHz, DMSO-d_6, ppm): δ 8.58 (1H, s, H-2‴), 8.20 (1H, s, H-5″), 8.08 (1H, d, J = 2.50 Hz, H-5‴), 7.87 (1H, dd, J = 9.00 Hz, J' = 2.50 Hz, H-7‴), 7.73 (1H, d, J = 9.00 Hz, H-8‴), 7.55 (2H, d, J = 7.50 Hz, H-2′, H-6′), 7.42 (1H, d, J = 15.50 Hz, H-3), 7.32 (2H, d, J = 8.00 Hz, H-3′, H-5′), 6.44 (1H, d, J = 15.50 Hz, H-2), 5.58 (2H, s, NC$\underline{H}_2$Ph), 5.27 (2H, s, C$\underline{H}_2$NCO). ^{13}C NMR (125 MHz, DMSO-d_6, ppm): δ 159.42, 148.88, 147.14, 142.92, 137.99, 137.43, 135.23, 135.09, 131.95, 130.06, 129.05, 128.30, 125.53, 124.36, 123.32, 120.11, 52.97, 41.70. HRMS (ESI) m/z calculated for: $C_{21}H_{17}ClN_6O_3$, $[M - H]^-$ 435.0972, 437.0943. Found, 435.0981, 437.0965.

2.2.5 (*E*)-3-(4-((4-((6-Fluoro-4-oxoquinazolin-3(4*H*)-yl) methyl)-1*H*-1,2,3-triazol-1-yl)methyl)phenyl)-*N*-hydroxyacrylamide (11e). White solid; yield: 45%, mp: 228.4–229.5 °C. R_f = 0.40 (DCM : MeOH = 9 : 1). IR (KBr, cm^{-1}): 3258 (OH); 3034, 2923 (CH, arene); 2853 (CH, CH_2); 1664, 1620 (C=O); 1604 (C=C). ^{1}H NMR (500 MHz, DMSO-d_6, ppm): δ 8.55 (1H, s, H-2‴), 8.20 (1H, s, H-5″), 7.83 (1H, dd, J = 8.75 Hz, H-5‴), 7.79 (1H, dd, J = 9.25 Hz, J' = 5.25 Hz, H-8‴), 7.73 (1H, td, J = 8.50 Hz, J' = 3.00 Hz, H-7‴), 7.55 (2H, d, J = 7.50 Hz, H-2′, H-6″), 7.42 (1H, d, J = 15.50 Hz, H-3), 7.33 (2H, d, J = 8.00 Hz, H-3′, H-5′), 6.46 (1H, d, J = 16.00 Hz, H-2), 5.59 (2H, s, NC$\underline{H}_2$Ph), 5.28 (2H, s, C$\underline{H}_2$NCO). ^{13}C NMR (125 MHz, DMSO-d_6, ppm): δ 162.98, 160.76 (J_{C-F} = 244.63 Hz), 147.88, 145.31, 142.98, 137.99, 137.43, 135.24, 130.71, 130.65, 129.05, 128.30, 124.36, 123.44 (J_{C-F} = 24.25 Hz), 123.38, 120.13, 111.21 (J_{C-F} = 23.38 Hz), 52.97, 41.62. HRMS (ESI) m/z calculated for: $C_{21}H_{17}FN_6O_3$, $[M - H]^-$ 419.1268. Found, 419.1274.

2.2.6 (*E*)-3-(4-((4-((7-Fluoro-4-oxoquinazolin-3(4*H*)-yl) methyl)-1*H*-1,2,3-triazol-1-yl)methyl)phenyl)-*N*-hydroxyacrylamide (11f). White solid; yield: 46%, mp: 225.5–226.8 °C. R_f = 0.40 (DCM : MeOH = 9 : 1). IR (KBr, cm^{-1}): 3231 (OH); 3060, 2921 (CH, arene); 2851 (CH, CH_2); 1664, 1619 (C=O); 1605, 1573 (C=C). ^{1}H NMR (500 MHz, DMSO-d_6, ppm): δ 8.61 (1H, s, H-2‴), 8.21 (1H, s, H-5″), 8.20 (1H, s, H-8‴), 7.56 (2H, d, J = 7.50 Hz, H-2′, H-6′), 7.50 (1H, d, J = 9.50 Hz, H-5‴), 7.43 (1H, d, J = 16.00 Hz, H-3), 7.42 (1H, d, J = 9.00 Hz, H-6‴), 7.34 (2H, d, J = 7.50 Hz, H-3′, H-5′), 6.46 (1H, d, J = 16.00 Hz, H-2), 5.59 (2H, s, NC$\underline{H}_2$Ph), 5.27 (2H, s, C$\underline{H}_2$NCO). ^{13}C NMR (125 MHz, DMSO-d_6, ppm): δ 167.13, 162.42 (J_{C-F} = 266.25 Hz), 159.72, 150.61 (J_{C-F} = 13.38 Hz), 149.80, 143.04, 138.03, 137.45, 135.26, 129.76 (J_{C-F} = 10.88 Hz), 129.06, 128.31, 124.35, 120.14, 119.15, 116.27 (J_{C-F} = 23.63 Hz), 112.89 (J_{C-F} = 21.63 Hz), 53.00, 41.56. HRMS (ESI) m/z calculated for: $C_{21}H_{17}FN_6O_3$, $[M - H]^-$ 419.1268. Found, 419.1270.

2.2.7 (*E*)-3-(4-((4-((6-Bromo-4-oxoquinazolin-3(4*H*)-yl) methyl)-1*H*-1,2,3-triazol-1-yl)methyl)phenyl)-*N*-hydroxyacrylamide (11g). White solid; yield: 43%, mp: 245.9–247.3 °C. R_f = 0.44 (DCM : MeOH = 9 : 1). IR (KBr, cm^{-1}): 3391 (NH), 3204 (OH); 3060, 3000 (CH, arene); 3365 (CH, CH_2); 1663 (C=O); 1601, 1553, 1514 (C=C). ^{1}H NMR (500 MHz, DMSO-d_6, ppm): δ 8.60 (1H, s, H-2‴), 8.22 (1H, s, H-5″), 8.22 (1H, s, H-5‴), 7.99 (1H, d, J = 8.50 Hz, H-7‴), 7.66–7.54 (3H, m, H-2′, H-6′, H-8‴), 7.42 (1H, d, J = 16.00 Hz, H-3), 7.33–7.29 (m, 2H, H-3′, H-5′), 6.45 (1H, d, J = 16.00 Hz, H-2), 5.58 (2H, s, NC$\underline{H}_2$Ph), 5.26 (2H, s, C$\underline{H}_2$NCO). ^{13}C NMR (125 MHz, DMSO-d_6, ppm): δ 159.30, 149.00, 147.41, 142.93, 138.02, 137.81, 137.44, 135.23, 130.19, 129.05, 128.91, 128.64, 128.32, 124.36, 123.67, 120.14, 52.98, 41.73. HRMS (ESI) m/z calculated for: $C_{21}H_{17}BrN_6O_3$, $[M - H]^-$ 479.0467, 481.0447. Found, 479.0468, 481.0456.

2.2.8 (*E*)-3-(4-((4-((7-Bromo-4-oxoquinazolin-3(4*H*)-yl) methyl)-1*H*-1,2,3-triazol-1-yl)methyl)phenyl)-*N*-hydroxyacrylamide (11h). White solid; yield: 43%, mp: 241.1–242.7 °C. R_f = 0.45 (DCM : MeOH = 9 : 1). IR (KBr, cm^{-1}): 3220 (OH); 3068, 3012 (CH, arene); 1664 (C=O); 1596, 1551, 1513 (C=C). ^{1}H NMR (500 MHz, DMSO-d_6, ppm): δ 8.59 (1H, s, H-2‴), 8.20 (1H, s, H-5″), 8.07 (1H, d, J = 8.50 Hz, H-5‴), 7.92 (1H, d, J = 1.50 Hz, H-8‴), 7.72 (1H, dd, J = 8.50 Hz, J' = 2.0 Hz, H-6‴), 7.54 (2H, d, J = 8.00 Hz, H-2′, H-6′), 7.41 (1H, d, J = 16.00 Hz, H-3), 7.32 (2H, d, J = 8.00 Hz, H-3′, H-5′), 6.45 (1H, d, J = 15.50 Hz, H-2), 5.58 (2H, s, NC$\underline{H}_2$Ph), 5.25 (2H, s, C$\underline{H}_2$NCO). ^{13}C NMR (125 MHz, DMSO-d_6, ppm): δ 162.98, 159.95, 149.80, 149.55, 142.94, 137.92, 137.41, 135.25, 130.73, 130.00, 129.05, 128.66, 128.53, 128.29, 124.36, 121.20, 120.18, 52.97, 41.65. HRMS (ESI) m/z calculated for: $C_{21}H_{17}BrN_6O_3$, $[M - H]^-$ 479.0467, 481.0447. Found, 479.0476, 481.0390.

2.2.9 (*E*)-*N*-Hydroxy-3-(4-((4-((6-iodo-4-oxoquinazolin-3(4*H*)-yl)methyl)-1*H*-1,2,3-triazol-1-yl)methyl)phenyl) acrylamide (11i). White solid; yield: 50%, mp: 263.4–265.3 °C. R_f = 0.46 (DCM : MeOH = 9 : 1). IR (KBr, cm^{-1}): 3365 (NH), 3202 (OH); 3121, 3001 (CH, arene); 2856 (CH, CH_2); 1663 (C=O); 1603, 1551 (C=C). ^{1}H NMR (500 MHz, DMSO-d_6, ppm): δ 8.69 (1H, s, H-2‴), 8.51 (1H, d, J = 2.00 Hz, H-5‴), 8.30 (1H, s, H-5″), 8.23 (1H, dd, J = 8.75 Hz, J' = 1.75 Hz, H-7‴), 7.65 (2H, d, J = 8.00 Hz, H-2′, H-6′), 7.59 (1H, d, J = 8.50 Hz, H-8‴), 7.52 (1H, d, J = 16.00 Hz, H-3), 7.43 (2H, d, J = 8.00 Hz, H-3′, H-5′), 6.57 (1H, d, J = 16.00 Hz, H-2), 5.68 (2H, s, NC$\underline{H}_2$Ph), 5.36 (2H, s, C$\underline{H}_2$NCO). ^{13}C NMR (125 MHz, DMSO-d_6, ppm): δ 162.96, 159.10, 149.03, 147.68, 143.31, 142.96, 137.93, 137.41, 135.25, 134.81, 129.93, 129.04, 128.31, 124.34, 123.83, 120.19, 92.82, 52.97, 41.71. HRMS (ESI) m/z calculated for: $C_{21}H_{17}IN_6O_3$, $[M - H]^-$ 527.0329. Found, 527.0335.

3. Results and discussions

3.1. Chemistry

The synthesis of the target *N*-hydroxybenzamides incorporating a 4-oxoquinazoline core was accomplished through a five-step synthetic pathway, as depicted in Scheme 1. The sequence began with the azidation of bromo-ester using sodium azide in methanol under reflux conditions. After solvent removal and extraction, a white-to-yellowish liquid was obtained in good

yield. This step efficiently introduced the azide functionality, setting the stage for subsequent transformations. Next, quinazoline-4(3*H*)-one derivatives (**4a–i**) were synthesized *via* the Niementowski reaction, in which anthranilic acid or its derivatives were cyclized with excess formamide at approximately 120 °C. Upon completion, the reaction mixture was poured into a sodium bicarbonate solution to neutralize residual acidic components, resulting in a purer product. The precipitate was filtered, washed with water, and dried to afford the desired intermediates without further purification. This one-step cyclization provided an efficient and high-yielding approach to constructing the quinazoline core. In the next step, the *N*-propargylation of **4a–i** using propargyl bromide, K_2CO_3, and KI in acetone under reflux produced intermediates **5a–i** in quantitative yields. This transformation was crucial for introducing the terminal alkyne moiety, which served as a key handle for the subsequent cycloaddition reaction. The copper(I)-catalyzed azide–alkyne cycloaddition (CuAAC) was then carried out by reacting propargyl intermediates **5a–i** with compound **2** in acetonitrile under reflux for 3 hours in the presence of CuI. This enabled the regioselective formation of 1,2,3-triazole-linked products (**6a–i**). Following alkaline work-up and solvent extraction, yellow solids were obtained in good yields, confirming the successful introduction of the triazole scaffold. Finally, the hydrolysis of esters **6a–i** to the target *N*-hydroxybenzamides **7a–i** was achieved using hydroxylamine hydrochloride in a methanol-DMF mixture under basic conditions (NaOH, pH 11) at 0 °C to minimize side reactions. Acidification with 5% HCl facilitated precipitation of the hydroxamic acid derivatives. The pure products were obtained by recrystallization in a methanol–water mixture, affording the final compounds **7a–i** in good yields (42–52%).

The target *N*-hydroxypropenamides incorporating quinazoline-4(3*H*)-one (**11a–i**) were synthesized using a strategy analogous to that employed for **7a–i**. However, for **11a–i**, methyl (*E*)-4-bromomethylcinnamate was employed instead of methyl 4-bromomethylbenzoate, as illustrated in Scheme 2. The reactions proceeded under similar conditions. Compounds **31a–c** and **33a–c** were obtained at an acceptable yields, ranging from 40–51% (see ESI† for copy of IR, MS, ^{1}H NMR, and ^{13}C NMR).

Table 1 Inhibition of HDAC activity and cytotoxicity of the synthesized compounds against several cancer cell lines

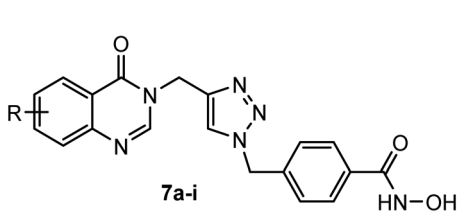

7a-i

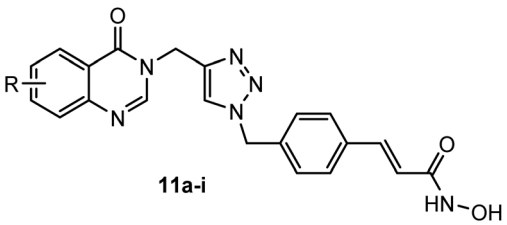

11a-i

Cpd	R	M_W	log P^a	HDAC (Hela extract) inhibiton ($IC_{50}{}^b$, μM)	Cytotoxicity ($IC_{50}{}^b$, μM)/cell lines[c]		
					SW620	MDA-MB-231	MRC-5
7a	–H	376.38	2.00	0.262	9.21 ± 0.72	14.07 ± 2.67	48.49 ± 6.23
7b	6-CH_3	390.40	2.49	0.425	43.11 ± 4.55	46.54 ± 12.62	165.80 ± 30.56
7c	7-CH_3	390.40	2.49	0.146	7.34 ± 0.94	7.05 ± 0.16	23.55 ± 4.82
7d	6-Cl	410.82	2.56	0.217	3.64 ± 0.31	3.64 ± 1.66	11.86 ± 1.43
7e	6-F	394.37	2.16	0.263	5.87 ± 1.55	7.99 ± 3.65	36.32 ± 6.57
7f	7-F	394.37	2.16	0.513	8.23 ± 2.04	7.47 ± 0.13	12.86 ± 2.40
7g	6-Br	455.27	2.83	0.188	20.80 ± 5.32	15.81 ± 1.32	44.88 ± 8.46
7h	7-Br	455.27	2.83	0.142	3.77 ± 1.87	4.38 ± 1.33	7.18 ± 1.94
7i	6-I	502.27	3.36	0.337	5.52 ± 1.04	4.56 ± 1.36	9.20 ± 4.52
11a	–H	402.41	2.34	0.958	5.07 ± 2.92	7.19 ± 0.95	36.70 ± 29.97
11b	6-CH_3	416.44	2.83	0.571	9.82 ± 2.46	9.71 ± 0.55	26.71 ± 12.01
11c	7-CH_3	416.44	2.83	0.939	11.74 ± 4.39	15.27 ± 3.94	48.10 ± 1.80
11d	6-Cl	436.86	2.90	0.234	3.15 ± 0.33	4.31 ± 0.14	20.65 ± 11.18
11e	6-F	420.40	2.50	0.463	4.57 ± 3.54	4.45 ± 2.05	12.63 ± 5.40
11f	7-F	420.40	2.50	0.464	5.34 ± 0.76	7.17 ± 1.99	15.04 ± 5.19
11g	6-Br	481.31	3.17	0.635	9.16 ± 0.08	9.07 ± 0.42	49.81 ± 29.68
11h	7-Br	481.31	3.17	0.360	5.73 ± 0.76	5.55 ± 0.18	56.08 ± 25.48
11i	6-I	528.31	3.70	1.028	28.48 ± 8.19	17.39 ± 6.11	73.01 ± 12.73
SAHA[d]		264.33	1.79	0.159	2.08 ± 0.35	3.75 ± 1.15	4.58 ± 1.09
ADR[e]		543.53	−1.34	—	0.56 ± 0.10	1.20 ± 0.24	0.42 ± 0.15

[a] Calculated by ChemDraw 16.0 software. [b] The concentration (μM) of compounds that produces a 50% reduction in enzyme activity or cell growth. [c] Cell lines: SW620: colon cancer, MDA-MB-231: breast cancer, MRC5: human fetal lung fibroblast cells. [d] SAHA: suberoylanilide hydroxamic acid, a positive control. [e] ADR: adriamycin, a positive control. The screenings were performed simultaneously with the compound sets published in the ref. 30.

3.2. Bioactivity

The cytotoxic effects of the synthesized compounds were investigated across three representative cell lines: SW620 (human colorectal adenocarcinoma), MDA-MB-231 (human triple-negative breast cancer), and MRC-5 (non-malignant human lung fibroblasts). Suberoylanilide hydroxamic acid (SAHA) was used as a reference compound (Table 1).

The synthesized quinazoline-based hydroxamic acids were evaluated for their HDAC inhibitory activity using nuclear extracts from HeLa cells. In general, the *N*-hydroxybenzamide derivatives (**7a–i**) demonstrated stronger HDAC inhibition compared to their *N*-hydroxypropenamide counterparts (**11a–i**). Among them, compound **7h** (7-Br) exhibited the most potent HDAC inhibition, with an IC_{50} value of 0.142 μM, followed by **7c** (7-CH_3, IC_{50} = 0.146 μM). These two compounds are the only ones that exhibit HDAC inhibitory activity comparable to the positive control, SAHA.

In the *N*-hydroxybenzamide series, structural modifications at positions 6 and 7 of the quinazoline core significantly influenced HDAC inhibitory activity. For the CH_3- and Br-substituted derivatives, substitution at position 7 resulted in stronger HDAC inhibition compared to the corresponding 6-substituted analogs. However, this trend was reversed in the fluorinated derivatives, where the 6-F derivative (**7e**) exhibited superior HDAC inhibition over its 7-F counterpart (**7f**), with IC_{50} values of 0.263 μM and 0.513 μM, respectively. A similar structure–activity relationship was observed in the *N*-hydroxypropenamide series, though with some notable exceptions. Bromo substitution at position 7 continued to enhance HDAC inhibition relative to position 6, as seen in **11h** (IC_{50} = 0.360 μM) *versus* **11g** (IC_{50} = 0.635 μM). However, the methyl-substituted analogs exhibited a reversed trend compared to the *N*-hydroxybenzamide series. Additionally, fluoro substitutions at positions 6 and 7 showed minimal impact on HDAC inhibition, as observed in **11e** (6-F) and **11f** (7-F). The

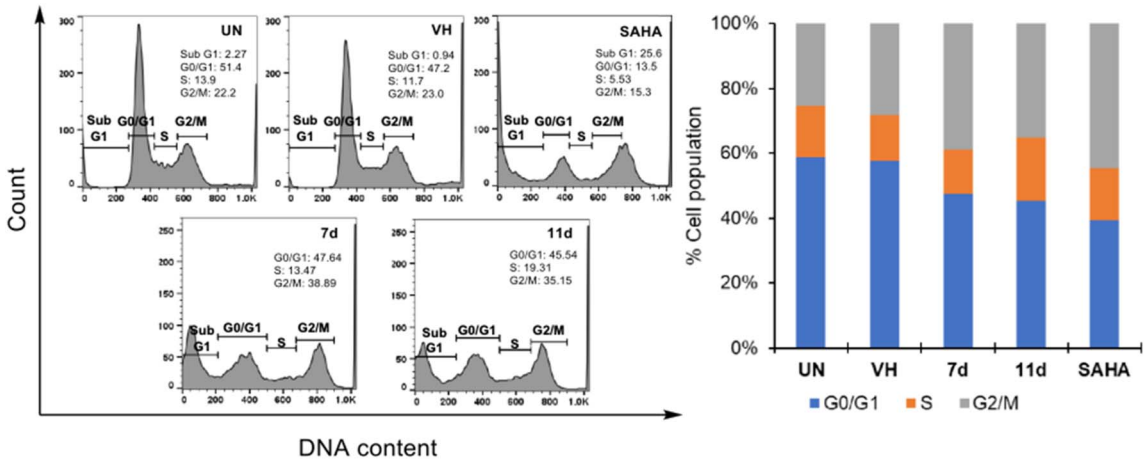

Fig. 3 Cell cycle analysis of representative compounds **7d** and **11d**. UN: untreated, VH: vehicle (DMSO 0.05%). Data was represented as histograms (left) and bar graphs (right).

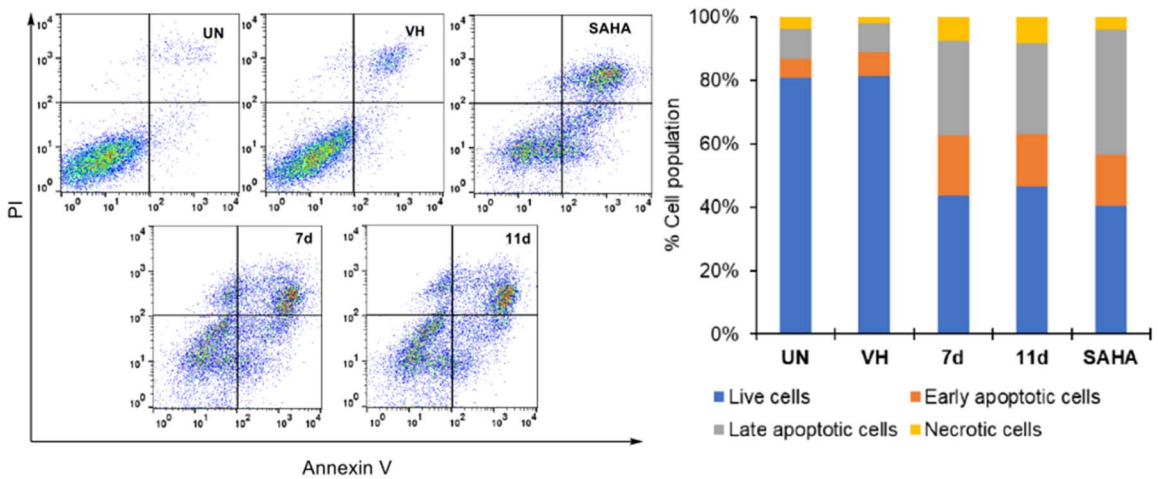

Fig. 4 Apoptosis (Annexin V/PI) analysis of representative compounds **7d** and **11d**. UN: untreated, VH: vehicle (DMSO 0.05%). Data was represented as histograms (left) and bar graphs (right).

introduction of an iodo substituent at position 6 led to a slight reduction in HDAC inhibition, with IC_{50} values of 0.337 μM (**7i**) and 0.262 μM (**7a**) in the *N*-hydroxybenzamide series and 1.028 μM (**11i**) and 0.958 μM (**11a**) in the *N*-hydroxypropenamide series. In contrast, chloro substitution at position 6 slightly enhanced HDAC inhibition in the *N*-hydroxybenzamide series (IC_{50} = 0.217 μM for **7d** *vs.* 0.262 μM for **7a**) but resulted in a marked increase in HDAC inhibitory potency in the *N*-hydroxypropenamide series (IC_{50} = 0.234 μM for **11d** *vs.* 0.958 μM for **11a**). These findings emphasize the crucial role of halogen substitution patterns in modulating HDAC inhibition and provide valuable insights for further optimization of quinazoline-based HDAC inhibitors. When comparing the *N*-hydroxybenzamide derivatives with the 4-oxoquinazoline scaffold previously reported by our research group,[16] it was observed that introducing a triazole ring enhanced HDAC inhibitory activity in the corresponding derivatives. Specifically, compounds bearing the same substituents on the quinazoline core exhibited increased potency when the triazole moiety was incorporated. This suggests that the presence of the triazole ring within the CU segment contributes positively to HDAC inhibition, possibly by improving interactions within the active site or increasing binding stability. In contrast, this trend was not observed for the *N*-hydroxypropenamide derivatives. In fact, the introduction of the triazole group in this series appeared to reduce HDAC inhibitory activity. A plausible explanation is that the triazole moiety may impose steric or conformational hindrance that disrupts the optimal orientation or interaction of the 4-oxoquinazoline CAP group with residues located at the rim of the HDAC binding pocket. This highlights the scaffold-

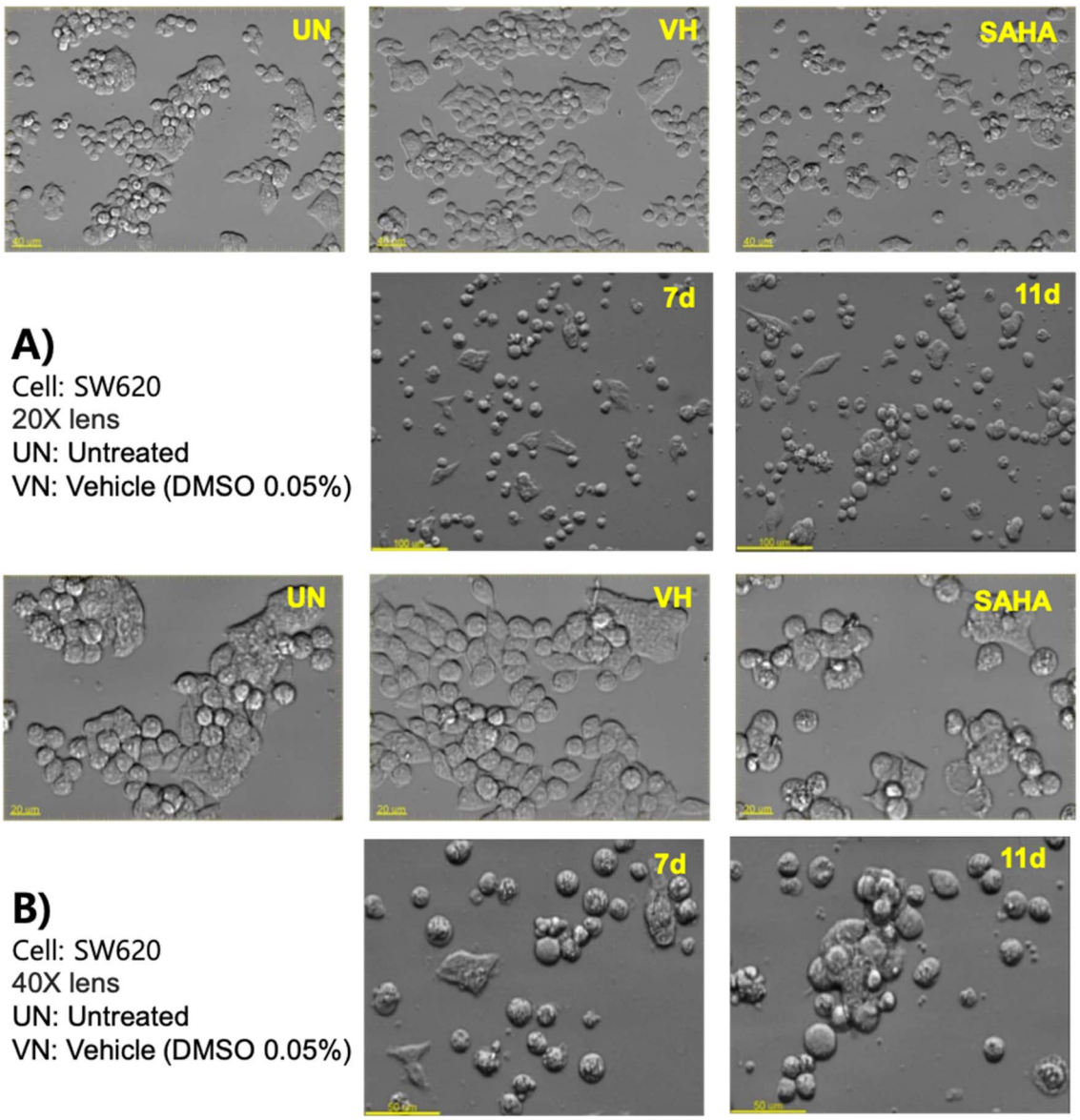

Fig. 5 Morphology changes of cells treated with representative compounds **7d** and **11d**. The cells were photographed using an imaging device: Biostation with 20× lens (A) or 40× lens (B).

dependent effect of triazole incorporation and suggests that its benefits are context-specific within the chemical architecture of HDAC inhibitors.

In terms of cytotoxicity, the *N*-hydroxypropenamide derivatives generally showed slightly stronger antiproliferative effects against the tested cancer cell lines (SW620 and MDA-MB-231) than the *N*-hydroxybenzamide series. Among the tested compounds, **7d** (6-Cl) showed the highest cytotoxic activity, with IC_{50} values of 3.64 ± 0.31 μM (SW620) and 3.64 ± 1.66 μM (MDA-MB-231). The introduction of a chlorine atom at the 6-position significantly enhanced anticancer activity compared to other halogens. Similarly, **11d** (6-Cl, IC_{50} = 3.15 ± 0.33 μM for SW620, 4.31 ± 0.14 μM for MDA-MB-231) also exhibited potent cytotoxicity, highlighting the positive impact of cloro substitution. In the *N*-hydroxybenzamide series, methyl substitution at position 7 (**7c**) resulted in greater cytotoxic activity compared to its 6-substituted counterpart (**7b**). However, this trend was completely reversed in the *N*-hydroxypropenamide series, where the 6-methyl derivative (**11b**) exhibited stronger cytotoxicity than the 7-methyl analog (**11c**). A notable trend was observed when comparing 6-halogenated and 7-halogenated derivatives: 7-Br (**7h**, **11h**) exhibited stronger anticancer activity than 6-Br (**7g**, **11g**), whereas the 6-F derivative (**7e**, **11e**) was more potent than the 7-F derivative (**7f**, **11f**). These findings suggest that the position of halogen substitution on the quinazoline scaffold plays a critical role in cytotoxic activity.

To evaluate the selectivity of the synthesized compounds, their cytotoxicity was assessed against normal human lung fibroblast cells (MRC-5). The majority of the derivatives exhibited significantly higher IC_{50} values for MRC-5 than for cancer cell lines, indicating selective toxicity toward cancer cells. For example, **11d** (6-Cl) showed an IC_{50} of 20.65 ± 11.18 μM against MRC-5, while its IC_{50} values for SW620 and MDA-MB-231 were 3.15 ± 0.33 μM and 4.31 ± 0.14 μM, respectively. Similarly, the highly cytotoxic compounds **11g** (6-Br) and **11h** (7-Br) exhibited IC_{50} values of 8.41 ± 1.29 μM and 10.15 ± 1.98 μM against MDA-MB-231, while their IC_{50} values for MRC-5 were much higher (48.01 ± 29.68 μM for **11g**, 73.01 ± 12.73 μM for **11h**).

SAHA (suberoylanilide hydroxamic acid), a clinically approved HDAC inhibitor, was used as a reference compound in this study. SAHA exhibited an HDAC IC_{50} value of 0.159 μM and cytotoxic IC_{50} values of 2.08 ± 0.35 μM (SW620), 3.75 ± 1.15 μM (MDA-MB-231), and 4.58 ± 1.09 μM (MRC-5). Compared to SAHA, most synthesized compounds demonstrated weaker HDAC inhibition, with IC_{50} values ranging from 0.142 to 0.958 μM, indicating that the quinazolinone-based hydroxamic acids exhibit HDAC inhibitory potential but require further optimization for enhanced potency. Although the synthesized compounds did not surpass SAHA in terms of HDAC inhibition, some derivatives, such as **7d** and **11d**, exhibited comparable or

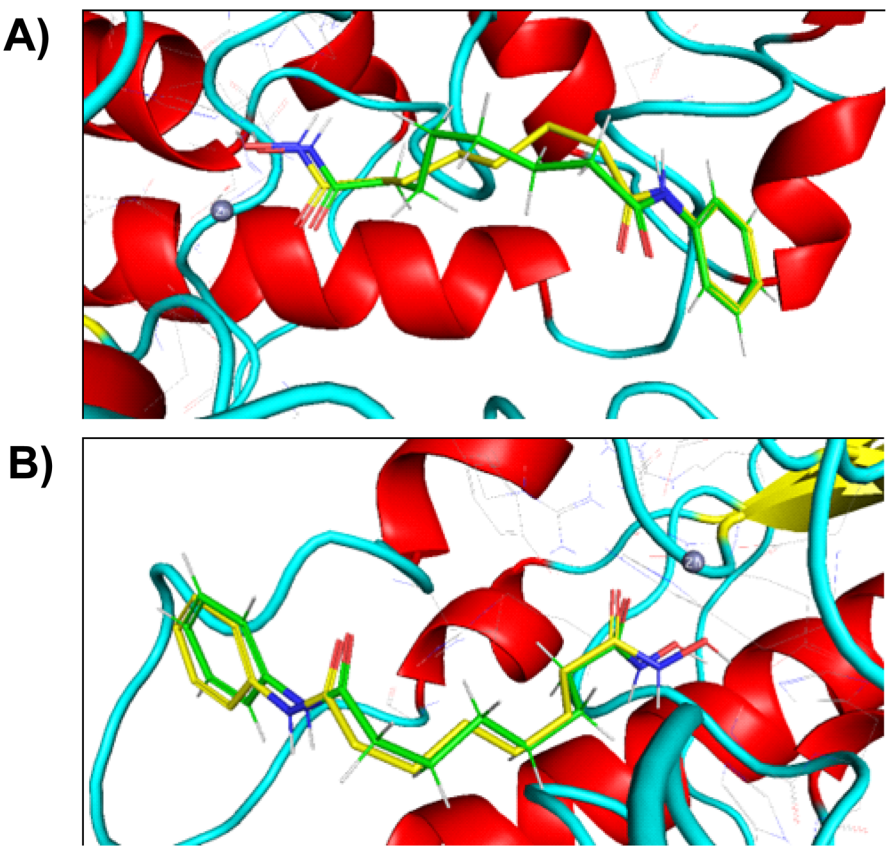

Fig. 6 (A) Re-docking simulation in HDAC2; (B) re-docking simulation in HDAC6. Co-crystallized and re-docked ligand were presented in yellow and green respectively.

superior cytotoxic activity against cancer cell lines while maintaining selectivity for cancer cells.

Based on their potent HDAC inhibition and promising cytotoxicity against two human cancer cell lines, compounds **7d** and **11d** were selected for further investigation regarding their effects on cell cycle progression and apoptosis in SW620 colon cancer cells.

To assess cell cycle effects, flow cytometry analysis was performed following 24-hour treatment with **7d**, **11d**, and SAHA at 5 μM. The results revealed that SAHA, **7d**, and **11d** all induced G2/M phase cell cycle arrest; however, the effect was less pronounced for **7d** and **11d** compared to SAHA (Fig. 3). Next, the pro-apoptotic effects of **7d** and **11d** were evaluated using an Annexin V-FITC/PI dual-staining assay. After 24-hour treatment at 5 μM, both **7d** and **11d** significantly induced early and late apoptosis, with early apoptosis levels exceeding those observed with SAHA (Fig. 4). Morphological changes in SW620 cells were also examined after 24-hour treatment at 5 μM. Microscopic

Table 2 Docking results of compounds **7a–i**, **11a–i** and SAHA against HDAC2, 3, and 6

HDAC2					HDAC2				
			Distance[b] to Zn^{2+}					Distance[b] to Zn^{2+}	
Cpd	*E*_score1[a]	*E*_score2[a]	–OH	=O	Cpd	*E*_score1[a]	*E*_score2[a]	–OH	=O
7a	−14.7415	−11.2474	2.10	2.39	**11a**	−14.6110	−11.7278	2.05	2.44
7b	−15.3315	−11.4803	2.10	2.39	**11b**	−13.1755	−11.7765	2.05	2.47
7c	−24.0177	−11.4284	2.06	2.48	**11c**	−16.2075	−11.8616	2.05	2.43
7d	−14.7250	−11.4298	2.10	2.39	**11d**	−13.6605	−11.7687	1.99	2.69
7e	−14.4214	−11.2914	2.10	2.39	**11e**	−13.9592	−11.6618	2.05	2.44
7f	−13.0715	−11.3161	2.06	2.48	**11f**	−12.5475	−11.7747	2.05	2.43
7g	−13.0726	−11.5423	2.10	2.39	**11g**	−13.3291	−11.8234	2.05	2.46
7h	−12.3480	−11.5099	2.06	2.48	**11h**	−13.2514	−11.9467	2.05	2.43
7i	−15.8183	−11.6253	2.10	2.40	**11i**	−13.7111	−11.9030	2.05	2.46
SAHA	−13.0934	−11.4267	2.00	2.59	SAHA	−13.0934	−11.4267	2.00	2.59
HDAC3					HDAC3				
			Distance[b] to Zn^{2+}					Distance[b] to Zn^{2+}	
Cpd	*E*_score1[a]	*E*_score2[a]	–OH	=O	Cpd	*E*_score1[a]	*E*_score2[a]	–OH	=O
7a	−11.5208	−9.2074	2.16	2.92	**11a**	−10.8044	−9.1889	2.17	3.34
7b	−11.3765	−9.1562	2.16	2.95	**11b**	−9.6986	−9.4308	2.18	3.36
7c	−10.7583	−9.3415	2.17	2.92	**11c**	−10.4324	−9.3624	2.17	3.35
7d	−11.6164	−8.9058	2.22	2.96	**11d**	−9.7457	−9.2929	2.18	3.37
7e	−10.4927	−9.1051	2.17	2.96	**11e**	−11.3826	−8.9359	2.19	3.42
7f	−10.6004	−9.1179	2.17	2.97	**11f**	−10.7830	−8.8864	2.16	3.43
7g	−11.3124	−9.1344	2.17	2.95	**11g**	−10.6771	−9.1639	2.20	3.36
7h	−13.4491	−8.9735	2.22	2.95	**11h**	−10.1990	−9.3909	2.17	3.34
7i	−10.5785	−9.1713	2.17	2.95	**11i**	−11.0488	−9.4501	2.17	3.34
SAHA	−16.0001	−10.0984	2.02	3.41	SAHA	−16.0001	−10.0984	2.02	3.41
HDAC6					HDAC6				
			Distance[b] to Zn^{2+}					Distance[b] to Zn^{2+}	
Cpd	*E*_score1[a]	*E*_score2[a]	–OH	=O	Cpd	*E*_score1[a]	*E*_score2[a]	–OH	=O
7a	−18.1526	−10.8626	2.17	2.27	**11a**	−15.1805	−11.3563	2.16	2.26
7b	−13.4690	−10.9952	2.14	2.29	**11b**	−15.8232	−11.6349	2.16	2.27
7c	−19.4791	−11.1576	2.15	2.27	**11c**	−14.1458	−11.6840	2.16	2.25
7d	−13.7657	−11.1777	2.09	2.32	**11d**	−16.1179	−11.5772	2.16	2.26
7e	−14.6419	−11.1076	2.09	2.32	**11e**	−14.2901	−11.4099	2.16	2.26
7f	−15.3496	−10.9426	2.08	2.34	**11f**	−13.1077	−11.4065	2.15	2.26
7g	−12.5861	−11.1793	2.08	2.32	**11g**	−15.2566	−11.6582	2.16	2.26
7h	−12.5662	−11.0516	2.10	2.29	**11h**	−16.7108	−11.6884	2.16	2.26
7i	−12.3915	−11.2112	2.09	2.33	**11i**	−15.4609	−11.6444	2.16	2.26
SAHA	−18.7663	−11.0001	2.08	2.30	SAHA	−18.7663	−11.0001	2.08	2.30

[a] The docking score (kcal mol^{-1}) calculated from the London (with refinement) and GBVI/WSA affinity scoring function from MOE software. [b] Distances (Å) from oxygen atoms (=O and –OH) of hydroxamic acid group to zinc ion.

analysis revealed that **7d** and **11d** induced characteristic apoptotic morphological alterations, including cell shrinkage and membrane blebbing, closely resembling the effects observed with SAHA (Fig. 5). Together, these findings highlight that while **7d** and **11d** exhibit comparable cytotoxicity to SAHA. The ability of **7d** and **11d** to induce apoptosis more effectively than SAHA suggests their potential as promising HDAC inhibitors with distinct anticancer properties.

3.3. Molecular docking studies

It was considerably desirable to conduct molecular docking simulations in order to further delve into the binding modes of our newly synthesized compounds. To validate the docking procedures applied, re-docking experiments were performed with two isozymes of histone deacetylase that consisted of HDAC2 (PDB ID: 4LXZ) and HDAC6 (PDB ID: 5EEI). Suberoylanilide hydroxamic acid or SAHA, a renowned pan-HDAC inhibitor, was the native ligand of each isoform. As shown in Fig. 6, SAHA confirmed a high degree of similarity with the co-crystallized ligand, since the values of root mean square deviation (RMSD) were both lower than 2.000 Å,[25] respectively 0.905 Å for HDAC2 and 0.429 Å for HDAC6 in particular. According to the obtained results, it was denoted that the following docking protocols would be promising for use in subsequent molecular docking studies.

Next steps, compounds **7a–i** and **11a–i** were docked into the active sites of three isoforms of HDAC, namely HDAC2 (PDB ID: 4LXZ), HDAC3 (PDB ID: 4A69) and HDAC6 (PDB ID: 5EEI). From that, the relationships between the structures of synthesized hydroxamic acid derivatives and their inhibitory activities could be highlighted. Docking results of two series were briefly summarized in Table 2. As indicated, our novel compounds participated in proper binding poses, comprising critical bidentate chelations, appropriate docking scores and relatively short distances (between the oxygen atoms of hydroxamate groups and the Zn^{2+} cation of the enzyme). In general, all 18 synthesized derivatives and SAHA were well fitted into the binding cavity of HDAC2 as they shared identical key interactions involving pivotal complexes with Zn^{2+} cation and three hydrogen bonds with His145, His146, Tyr308. Nonetheless, there existed several noticeable alterations in binding geometries between the two series. For instance, the benzamide linker associated with the 1,2,3-triazole ring showed numerous interactions such as hydrophobic contacts (with Leu276), π–alkyl stackings (with His146) and π–π interactions (with Phe210, Phe155) in most compounds of series **7a–i**; meanwhile, the cinnamamide moiety of **11a–i** facilitated van der Waals contacts with Asp104 and Leu276 residues. Likewise, the presence of 4-oxoquinazoline ring contributed to various interactions with His33 or Glu103 (in most of the compounds **11a–i**), or with His33, Glu103, Gln31 (in most of the compounds **7a–i**). On the other hand, SAHA displayed notably more interactions in comparison to all synthesized compounds as contacts with His33, Asp104, Phe155 (of the anilide ring) and with His183, His146, Phe155, Asp104, Phe210 (of the heptanamide moiety) were observed. The docking scores ranged from −11.2474 kcal mol^{-1} to −11.6253 kcal mol^{-1} for series **7a–i** and from −11.7278 kcal mol^{-1} to −11.9467 kcal mol^{-1} for series **11a–i**, whereas the estimated value of SAHA was −11.4267 kcal mol^{-1}. This suggested that compared to SAHA, compounds **7a–i** demonstrated comparable HDAC2 inhibitory activity while **11a–i** exhibited better inhibition potency against HDAC2. Similarly, the chelators of all ligands displayed identical interactions, including bidentate complexes with Zn^{2+} cation and hydrogen bonds with His573, His574, Tyr745

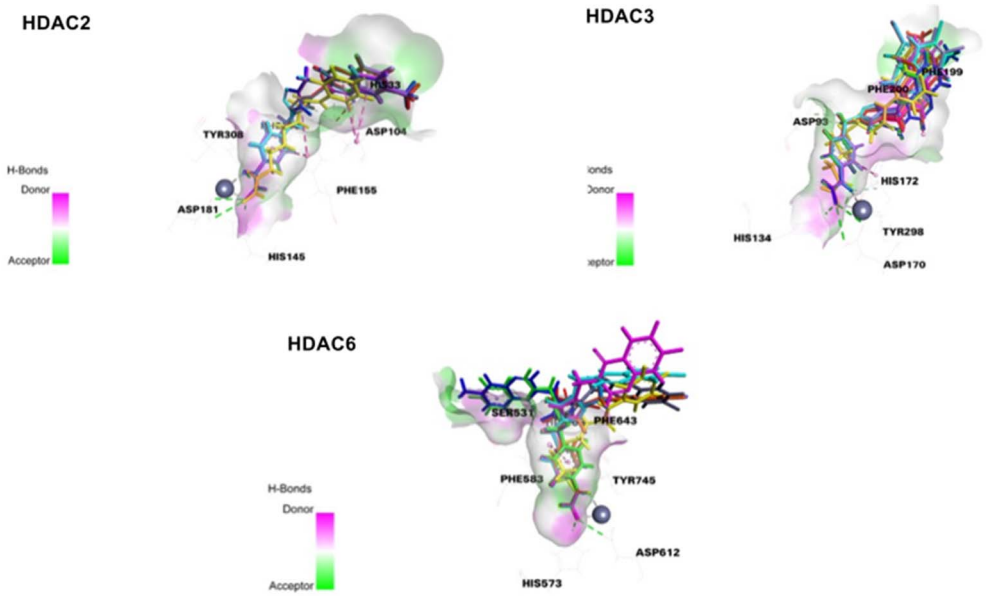

Fig. 7 Binding poses of compounds **7a–i** and SAHA into HDAC2, HDAC3, HDAC6. The ligands were coloured in green #00ff00 (**7a**), red #ff0000 (**7b**), blue #0000ff (**7c**), violet #aa55ff (**7d**), orange #ff5500 (**7e**), magenta #ff00ff (**7f**), sky blue #00aaff (**7g**), cyan #00ffff (**7h**), indigo gray #55557f (**7i**), yellow #ffff00 (SAHA) with respective RGB codes.

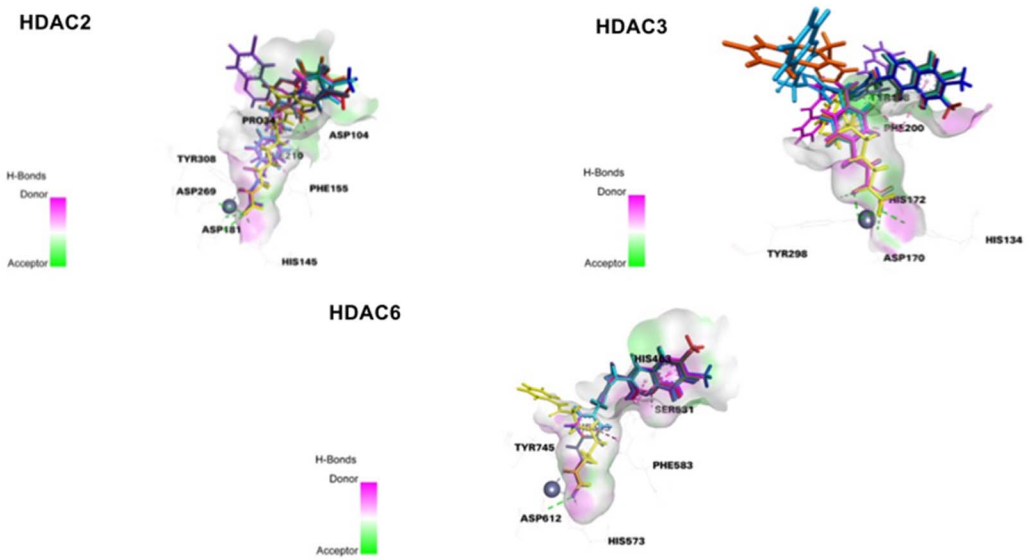

Fig. 8 Binding poses of compounds **11a–i** and SAHA into HDAC2, HDAC3, HDAC6. The ligands were coloured in green #00ff00 (**11a**), red #ff0000 (**11b**), blue #0000ff (**11c**), violet #aa55ff (**11d**), orange #ff5500 (**11e**), magenta #ff00ff (**11f**), sky blue #00aaff (**11g**), cyan #00ffff (**11h**), indigo gray #55557f (**11i**), yellow #ffff00 (SAHA) with respective RGB codes.

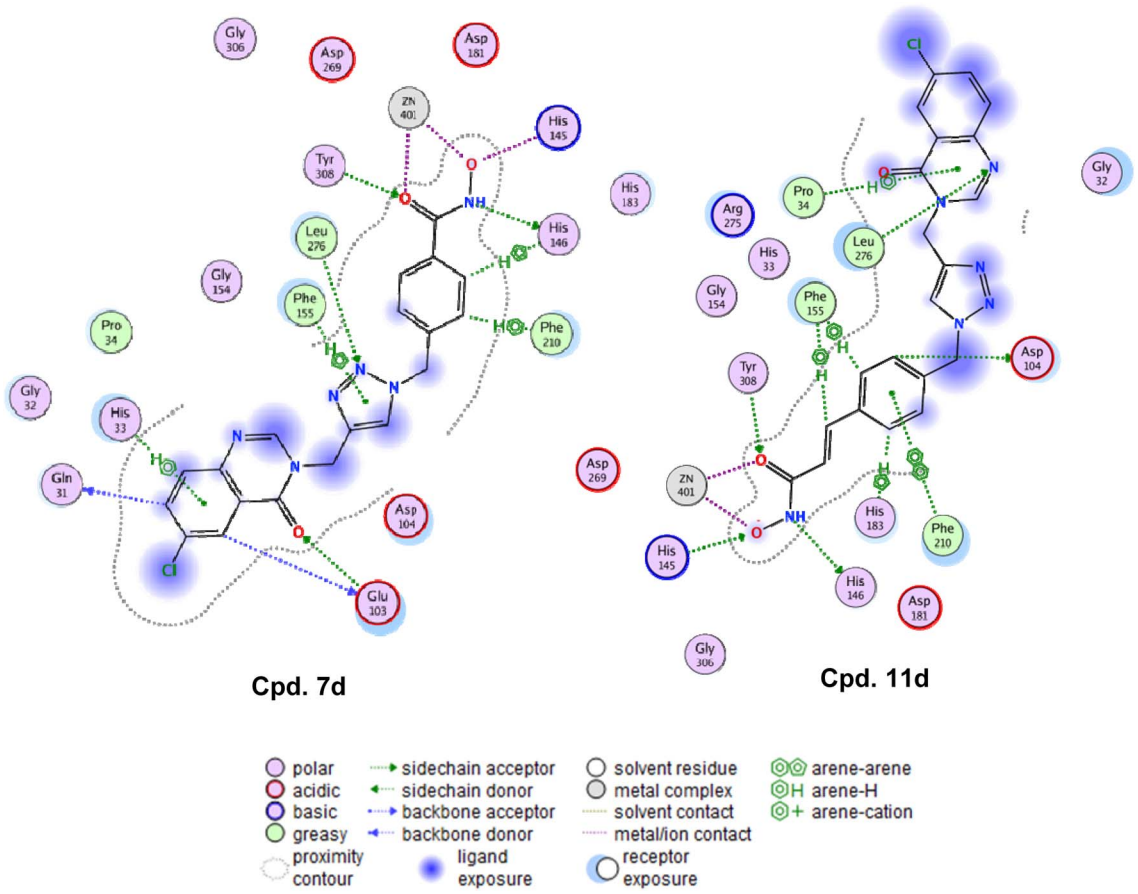

Fig. 9 2D presentation of the binding poses and interactions of compounds **7d** and **11d** in HDAC2 binding pocket.

residues upon docked into the binding domain of HDAC6. The cinnamamide moiety of **11a–i** was favourable for π–π stackings with Phe643, whereas the benzamide linker of **7a–i** was suitable for contacts towards Phe583 and Gly582. Although interactions of the 4-oxoquinazoline ring fluctuated, the four residues Ser531, Phe583, Asn457, Phe533 were most probably involved in

observed bonds of compounds **11a–i**. The heptanamide linker coupled with the anilide ring of SAHA showed a preference to express plentiful interactions, such as π–π stackings with Phe642 and π–alkyl contacts with His614, Phe643, His574. Many synthesized compounds, astonishingly, exhibited better docking scores compared with those of SAHA, recommending their stronger inhibition activity against HDAC6. In contrast, the designed ligands were anticipated to interact more weakly in relation to SAHA as HDAC3 inhibitors, since their calculated docking scores implied a diminishment in binding affinity. Based on the docking results, it could be implied that **7a–i** and **11a–i** adopted energetically and topologically good docking poses; however, they generally exhibited weaker inhibitory activity in comparison with SAHA as indicated by experimental results presented in Table 1. Inherent limitations of molecular docking approaches, including the lack of scoring functions capable of accurately evaluating specific types of protein-ligand complexes, might lead to discrepancies between docking outcomes and experimental data.[26] Despite these obstacles, *in silico* methods could provide valuable insights into the binding modes of designed ligands. Given the potential of HDAC6 as a prospective target for tumor treatment, such as colorectal cancer,[27] melanoma,[28] breast cancer,[29] our synthesized derivatives can serve as scaffolds for future optimizations of selective inhibitors with higher potency against HDAC6 isoform. Binding geometries of **7a–i** and **11a–i** were visualized in Fig. 7, 8 and 9.

4. Conclusions

In summary, we successfully synthesized and evaluated a series of quinazoline-based hydroxamic acids for HDAC inhibition and anticancer activity. These compounds demonstrated notable HDAC inhibitory potency, with *N*-hydroxybenzamide derivatives (**7a–i**) generally outperforming their *N*-hydroxypropenamide counterparts (**11a–i**). Compounds **7h** (7-Br) and **7c** (7-CH_3) emerged as the most potent HDAC inhibitors, exhibiting inhibitory activity comparable to that of the positive control, SAHA. Cytotoxicity studies revealed that the 6-Cl derivatives (**7d**, **11d**) showed the highest antiproliferative effects and selectivity toward cancer cells. Additionally, **7d** and **11d** effectively induced G2/M cell cycle arrest and apoptosis, highlighting their therapeutic potential. These findings underscore the significance of structural modifications in optimizing HDAC inhibition and anticancer activity. Further investigations, including *in vivo* studies and mechanistic insights, are warranted to advance these compounds as promising HDAC-targeting anticancer agents.

Data availability

The data supporting this article have been included as part of the ESI.†

Author contributions

N.-H. N and S.-B. H. proposed the work. N.-H. N, T. T. T, N. P. D, N. T. N, B. Q. C. and D. T. A. mainly developed the synthesis studies, S.-B. H, H. K. K, D. H. K, H. Y. K, and J. S. K. performed the biological testing assays. All authors read and approved the final manuscript.

Conflicts of interest

The authors report no conflict of interest.

Acknowledgements

We acknowledge the principal financial supports from the National Foundation for Science and Technology of Vietnam (NAFOSTED, Grant number 104.01-2023.17). The work was also partly supported by a grant funded by the Korean Government (KFRM RS-2024-00332516).

References

1 C. L. Miranda Furtado, *et al.*, Epidrugs: targeting epigenetic marks in cancer treatment, *Epigenetics*, 2019, **14**(12), 1164–1176.
2 N. Sengupta and E. Seto, Regulation of histone deacetylase activities, *J. Cell. Biochem.*, 2004, **93**(1), 57–67.
3 V. Davalos and M. Esteller, Cancer epigenetics in clinical practice, *Ca-Cancer J. Clin.*, 2023, **73**(4), 376–424.
4 M. Glozak and E. Seto, Histone deacetylases and cancer, *Oncogene*, 2007, **26**(37), 5420–5432.
5 E. Seto and M. Yoshida, Erasers of histone acetylation: the histone deacetylase enzymes, *Cold Spring Harbor Perspect. Biol.*, 2014, **6**(4), a018713.
6 O. Witt, *et al.*, HDAC family: What are the cancer relevant targets?, *Cancer Lett.*, 2009, **277**(1), 8–21.
7 F. R. Fritzsche, *et al.*, Class I histone deacetylases 1, 2 and 3 are highly expressed in renal cell cancer, *BMC Cancer*, 2008, **8**(1), 1–10.
8 W. Weichert, *et al.*, Class I histone deacetylase expression has independent prognostic impact in human colorectal cancer: specific role of class I histone deacetylases in vitro and in vivo, *Clin. Cancer Res.*, 2008, **14**(6), 1669–1677.
9 H. Adams, *et al.*, Class I histone deacetylases 1, 2 and 3 are highly expressed in classical Hodgkin's lymphoma, *Expert Opin. Ther. Targets*, 2010, **14**(6), 577–584.
10 I. Oehme, *et al.*, Histone deacetylase 8 in neuroblastoma tumorigenesis, *Clin. Cancer Res.*, 2009, **15**(1), 91–99.
11 B. Barneda-Zahonero and M. Parra, Histone deacetylases and cancer, *Mol. Oncol.*, 2012, **6**(6), 579–589.
12 R. Parveen, D. Harihar and B. P. Chatterji, Recent histone deacetylase inhibitors in cancer therapy, *Cancer*, 2023, **129**(21), 3372–3380.
13 M. Manal, *et al.*, Inhibitors of histone deacetylase as antitumor agents: A critical review, *Bioorg. Chem.*, 2016, **67**, 18–42.
14 D. A. Rodrigues, *et al.*, Histone deacetylases as targets for the treatment of neurodegenerative disorders: Challenges and future opportunities, *Med. Res. Rev.*, 2020, **40**(6), 2177–2211.
15 M. S. Nasrollahzadeh, *et al.*, Design, synthesis and biological evaluation of novel imidazole-based benzamide and

hydroxamic acid derivatives as potent histone deacetylase inhibitors and anticancer agents, *J. Mol. Struct.*, 2024, **1297**, 136951.

16 D. T. Hieu, *et al.*, Design, synthesis and evaluation of novel N-hydroxybenzamides/N-hydroxypropenamides incorporating quinazolin-4 (3H)-ones as histone deacetylase inhibitors and antitumor agents, *Bioorg. Chem.*, 2018, **76**, 258–267.

17 D. T. Anh, *et al.*, Design, synthesis and evaluation of novel indirubin-based N-hydroxybenzamides, N-hydroxypropenamides and N-hydroxyheptanamides as histone deacetylase inhibitors and antitumor agents, *Bioorg. Med. Chem. Lett.*, 2020, **30**(22), 127537.

18 P. Bertrand, Inside HDAC with HDAC inhibitors, *Eur. J. Med. Chem.*, 2010, **45**(6), 2095–2116.

19 S. Gatadi, T. V. Lakshmi and S. Nanduri, 4 (3H)-Quinazolinone derivatives: Promising antibacterial drug leads, *Eur. J. Med. Chem.*, 2019, **170**, 157–172.

20 M. M. Alam, 1, 2, 3-Triazole hybrids as anticancer agents: a review, *Arch. Pharm.*, 2022, **355**(1), 2100158.

21 E. Bonandi, *et al.*, The 1, 2, 3-triazole ring as a bioisostere in medicinal chemistry, *Drug Discovery Today*, 2017, **22**(10), 1572–1581.

22 G. Huang, *et al.*, Discovery of fast-acting dual-stage antimalarial agents by profiling pyridylvinylquinoline chemical space via copper catalyzed azide-alkyne cycloadditions, *Eur. J. Med. Chem.*, 2021, **209**, 112889.

23 N. Sun, *et al.*, Design and Synthesis of Triazole-Containing HDAC Inhibitors That Induce Antitumor Effects and Immune Response, *J. Med. Chem.*, 2023, **66**(7), 4802–4826.

24 P. C. Chen, *et al.*, Synthesis and structure–activity relationship of histone deacetylase (HDAC) inhibitors with triazole-linked cap group, *Bioorg. Med. Chem.*, 2008, **16**(9), 4839–4853.

25 D. Li, *et al.*, Acupuncture Therapy on Dementia: Explained with an Integrated Analysis on Therapeutic Targets and Associated Mechanisms, *J. Alzheimers Dis.*, 2023, **94**(s1), S141–s158.

26 A. Sacan, S. Ekins and S. Kortagere, Applications and limitations of in silico models in drug discovery, *Methods Mol. Biol.*, 2012, **910**, 87–124.

27 Y. Wen, *et al.*, HDAC6 inhibitor ACY-1215 enhances STAT1 acetylation to block PD-L1 for colorectal cancer immunotherapy, *Cancer Immunol. Immunother.*, 2024, **73**(1), 7.

28 S. k. R. Noonepalle, *et al.*, Cell therapy using ex vivo reprogrammed macrophages enhances antitumor immune responses in melanoma, *J. Exp. Clin. Cancer Res.*, 2024, **43**(1), 263.

29 D. Banik, *et al.*, HDAC6 Plays a Noncanonical Role in the Regulation of Antitumor Immune Responses, Dissemination, and Invasiveness of Breast Cancer, *Cancer Res.*, 2020, **80**(17), 3649–3662.

30 N. Q. Thang, N. T. Nga, J. S. Kim, H. K. Kim, J. Kim, J. S. Kang, T. T. Tung, D. T. M. Dung, D. T. Anh, S.-B. Han and N.-H. Nam, Design, synthesis and bioevaluation of novel N-heterocyclic hydroxamic acids as histone deacetylase inhibitors and their antitumor activity study, *New J. Chem.*, 2024, **48**, 19144–19166.